Wigner spectrum and coherent feedback control of continuous-mode single-photon states

Zhiyuan Dong[1], Lei Cui[1], Guofeng Zhang[1] and Hongchen Fu[2]

[1] Department of Applied Mathematics, The Hong Kong Polytechnic University, Hong Kong, China

[2] School of Physical Sciences and Technology, Shenzhen University, Shenzhen 518060, China

E-mail: Guofeng.Zhang@polyu.edu.hk

July 2016

Abstract. Normal ordering (Wick order) is commonly used in the analysis of quantum correlations. Unfortunately it can only give partial information for correlation analysis. For example, for a continuous-mode single-photon state (whose correlation function consists of two parts, one due to quantum vacuum noise and the other due to photon pulse shape), the normal ordering analysis simply ignores the contribution from the quantum white noise. In this paper, we propose to use Wigner spectrum to analyze single-photon states. We show Wigner spectrum is able to provide complete quantum correlation in time and frequency domains simultaneously. We demonstrate the effectiveness of the method by means of two examples, i.e., optical cavity (a passive system) and degenerate parametric amplifier (a non-passive system). Numerical simulations show that Wigner spectra are able to reveal the clear difference between the output states of these two systems driven by the same single-photon state. We also investigate how to use control methods to engineer photon pulse shapes of the output state of a quantum linear system in response to a single-photon state.

PACS numbers: 42.50.Ct, 02.30.Yy, 02.30.Nw, 02.70.Hm

Submitted to: *J. Phys. A: Math. Theor.*

(Some figures may appear in color only in the online journal)

1. Introduction

Single photons are fundamental resources for quantum communication [1, 2], quantum computing [3, Chapter 6.3], [4], quantum metrology [5, 6, 7], and quantum networks [8, 9, 10]. In contrast to single-mode photon states, continuous-mode photon states are closer to a real experimental environment in quantum information processing [11, 12, 13, 14]. In [15], the authors discussed efficient excitation of a two-level atom by a single-photon state. Both continuous-mode single-photon Fock state and continuous-mode single-photon coherent states are used as probes. And the effect of their temporal

pulse shapes (for example Gaussian, hyperbolic secant, rectangular, rising exponential and decaying exponential) on the excitation probability is studied. A theoretical framework is presented in [16] which describes the interaction between light wave packets of arbitrary spectral distribution functions and a quantum system. Master equations for the system and output field quantities (e.g., quadratures and photon flux) also have been discussed in this framework. Recently, an experiment has been conducted which demonstrated real-time measurement of a rising exponential single-photon wavepacket [17]. In this experiment, a single-mode optical parametric oscillator (OPO) with a built-in polarization beamsplitter is used to generate a signal photon of rising exponential pulse shape which is triggered by the idler photon measured by avalanche photodiode (APD). The quantum filters for an arbitrary quantum system driven by a continuous-mode single photon Fock state has be investigated in [18]. Two approaches are proposed, the non-markovian embedding technique [19] and the markovian embedding technique [20], and the latter discussed how to design a two-level system to generate a desired continuous-mode single-photon Fock state. The study in [19, 20] are extended in [16] to derive the master equations of an arbitrary quantum system driven by continuous-mode multi-photon Fock wave packets. Moreover, based on [19], the quantum filters of an arbitrary quantum system driven by a continuous-mode multi-photon state are derived in [21]. By applying the stochastic master equations to a cavity driven by a continuous-mode single-photon field, the conditional dynamics for the cross phase modulation in a doubly resonant cavity are analyzed in [22]. Based on a quantum stochastic model, some previous results are solved numerically, as well as different effects on the distribution of conditional phase shifts. Furthermore, the formalism is well suited to measurement-based feedback control [23]. Linear signals and systems theory has recently been proposed to study single-photon quantum signals, and the response of quantum linear systems driven by multi-channel single-photon input fields are investigated in [24]. It is shown that the steady-state output is in a single-photon state for a cavity driven by a single-photon input state, while this is not the case for a degenerate parametric amplifier (DPA). A class of photon-Gaussian states is defined which can describe the steady-state output state of the DPA. It has also been proved that the class of photon-Gaussian states are invariant in regard to quantum linear dynamics. Interestingly, single-photon states are special cases of photon-Gaussian states. A mathematical framework for analyzing the quantum linear systems' response to multi-photon states is presented in [25], where both the factorizable and unfactorizable wave packtes are treated. Particularly, a more general class of states represented by tensor is defined when the quantum linear system is driven by multi-photon input states.

The Wigner function (also called the Wigner quasiprobability distribution or the Wigner-Ville distribution) is firstly introduced by Eugene Wigner [26] and used to link the wave function to a probability distribution in phase space. The simplified scheme with randomly varied phase has been conducted in [27]. A phase-averaged Wigner function and diagonal elements of density matrix for a single-photon Fock state are reconstructed using the method of homodyne tomography. Since the exhibition of

negative values around the origin of phase space, the reconstructed Wigner function reflects the non-classical property of the single-photon state. In this case, experimental results, such as detection efficiency, minimum of Wigner function, are consistent with the theoretical evaluations. A continuous-wave (cw) laser was used in the experiment as light source to generate arbitrary superposition of Fock states in [28]. Those generated superposition states with wider bandwidth are applicable to the teleportation-based quantum operations. Particularly, a three photon Fock state $|3\rangle$, superpositions of Fock states $|1\rangle$ and $|3\rangle$, and $|0\rangle$ and $|3\rangle$ are generated in the experiments. Multiple areas of negativity of Wigner function are observed to verify the non-classical property of the generated states. An experimental technique of polychromatic optical heterodyne tomography is presented in [29] and nonvanishing imaginary parts have been added into the temporal mode function (TMF) to demonstrate the technique can reconstruct photon states with complex temporal modes. Both the real and imaginary components of a single-photon's temporal density matrix are considered by measuring the reduced autocorrelation matrix. In addition, the experimental temporal modes and their theoretical predictions are compared with several modulations.

The first goal of this paper is to use Wigner spectrum, the time-frequency variant of the Wigner function, to analyze the covariance functions for continuous-mode single-photon states. In most literature, correlations are calculated for normal ordered (Wick order) operators to avoid the delta function, see e.g. [30]. For example, the normal ordering of $\hat{a}(t)\hat{a}^\dagger(r)$ is $:\hat{a}(t)\hat{a}^\dagger(r):=\hat{a}^\dagger(r)\hat{a}(t)$. That is, the impulse function $\delta(t-r)$ has been thrown away. In our paper, instead of the partial information of the normal ordering term $:\hat{a}(t)\hat{a}^\dagger(r):$, we intend to present a direct analysis on $\hat{a}(t)\hat{a}^\dagger(r)$ in terms of the Wigner spectrum method, therefore keeping the complete information.

The problem of pulse-shaping of single-photon states has been investigated in [31]. The relation between input and output pulse shapes is derived in the frequency domain when the underlying system is an empty cavity. Quantum interface between optical and microwave fields is described by using a micromechanical resonator (MR) in [32]. The outputs of the local oscillator and the cavity are mixed by a beamsplitter and filtered output modes can be defined by proper temporal mode function of this oscillator. In the case of an even cat input state, the fidelity has been calculated and simulation results show that the proposed teleportation scheme has high quality. The response of quantum nonlinear systems to single-photon input states is presented in [33]. Particularly, the output states and pulse shapes for quantum two-level systems are derived explicitly in time and frequency domains. The input-output relation of pulse shapes is expressed by transfer function in [24]. The pulse-shaping problem in the case of quantum linear systems has also been discussed and can be implemented. A memory subsystem within a linear network is proposed in [34]. The memory system is decoupled from the optical field during the storage process while coupled to the field in the other processes. The zero-dynamic principle, that is, the output field for passive system must be vacuum, is emphasized for quantum memory problem. Recently, a complete framework with the temporal modes (TMs) of single-photon states is proposed in [14]. The definition

of temporal modes and its application in quantum information encoding are reviewed. Particularly, the quantum pulse gate (QPG), which is equivalent to a TM reshaper, is presented and the reshaping operation is given theoretically.

Along the above lines, the second goal of this paper is to show how to use coherent feedback control to engineer wave packets and Wigner spectra of single-photon states.

The rest of the article is organized as follows. Single-photon states, Wigner distribution and Wigner spectrum are briefly introduced in Section 2. Then Wigner spectrum for an optical cavity is characterized later, the changes of Wigner spectrum with respect to cavity decay rate and de-tuning are treated. In contrast to the cavity case, Wigner spectra for DPA are also presented in Section 3. In Section 4, the wave packets of several coupled systems are compared, together with the corresponding detection probabilities. Moreover, Wigner spectrum for a feedback network which contains a cavity and a beamsplitter is analyzed. Finally, Section 5 contains some concluding remarks.

2. Wigner spectrum for optical cavity

2.1. Single-photon states

Let $\hat{b}[\omega]$ be the annihilation operator for mode ω of the input field. $\hat{b}[\omega]$ and its adjoint operator $\hat{b}^\dagger[\omega]$ satisfy the singular commutation relation

$$\left[\hat{b}[\omega_1], \hat{b}^\dagger[\omega_2]\right] = \delta\left(\omega_1 - \omega_2\right). \tag{1}$$

Define an operator in the interaction picture

$$\hat{\mathbf{B}}(\xi) \triangleq \int_{-\infty}^{\infty} d\omega \ \xi^*[\omega]\hat{b}[\omega], \tag{2}$$

where $\|\xi\| \triangleq \int_{-\infty}^{\infty} d\omega \ \left|\xi[\omega]\right|^2 = 1$. A *continuous-mode single-photon Fock state* with the spectral pulse shape $\xi[\omega]$ is defined to be

$$\left|1_\xi\right\rangle \equiv \hat{\mathbf{B}}^\dagger(\xi)\left|0\right\rangle \triangleq \int_{-\infty}^{\infty} d\omega \ \xi[\omega]\hat{b}^\dagger[\omega]\left|0\right\rangle. \tag{3}$$

$\hat{b}^\dagger[\omega]$ is the creation operator of the light field, and thus $\hat{b}^\dagger[\omega]\left|0\right\rangle \equiv \left|1_\omega\right\rangle$ can be understood as photon generation at frequency ω, while the probability is given by $\left|\xi[\omega]\right|^2$. So the continuous-mode single-phton Fock state $\left|1_\xi\right\rangle$ can be interpreted as a photon coherently superposed over a continumn of frequency modes, with probability amplitudes given by the spectral density function $\xi[\omega]$. The Fourier transform of (3) gives the time-domain expresson of the single-photon Fock state, which is

$$\left|1_\xi\right\rangle = \int_{-\infty}^{\infty} dt \ \xi(t)\hat{b}^\dagger(t)\left|0\right\rangle. \tag{4}$$

Clearly, the time-domain counterpart of the commutation relation (1) is

$$\left[\hat{b}(t), \hat{b}^\dagger(r)\right] = \delta\left(t - r\right). \tag{5}$$

It is easy to show that the continuous-mode single-photon Fock state $|1_\xi\rangle$ has the following properties,

$$\left\langle 1_\xi|\hat{\mathbf{B}}^\dagger(\xi)|1_\xi\right\rangle = \left\langle 1_\xi|\hat{\mathbf{B}}(\xi)|1_\xi\right\rangle = 0, \tag{6}$$

and

$$\hat{\mathbf{B}}(\xi)\,|1_\xi\rangle = \|\xi\|^2 = 1. \tag{7}$$

Next we discuss *continuous-mode single-photon coherent states*, which can be defined to be, [13, Eq. (3.1)]

$$|\alpha_\xi\rangle \;=\; \exp\left(\alpha\hat{\mathbf{B}}(\xi)^\dagger - \alpha^*\hat{\mathbf{B}}(\xi)\right)|0\rangle \tag{8a}$$

$$\;=\; \exp\left(\int_{-\infty}^{\infty} d\omega\;\alpha\xi[\omega]\hat{b}^\dagger[\omega] - \int_{-\infty}^{\infty} d\omega\;(\alpha\xi[\omega])^*\hat{b}[\omega]\right)|0\rangle\,, \tag{8b}$$

where $\alpha = e^{i\theta}$ is a complex number. Clearly, by the Baker-Hausdorff formula, $|\alpha_\xi\rangle$ can be re-written as

$$|\alpha_\xi\rangle = \exp\left(-\frac{|\alpha|^2}{2}\right)\exp(\alpha\hat{\mathbf{B}}^\dagger(\xi)))\exp(-\alpha^*\hat{\mathbf{B}}(\xi))\,|0\rangle\,. \tag{9}$$

Consequently, we may express the continuous-mode single-photon coherent state in terms of continuous-mode number states, that is,

$$|\alpha_\xi\rangle = \exp\left(-\frac{|\alpha|^2}{2}\right)\sum_{n=0}^{\infty}\frac{\alpha^n}{\sqrt{n!}}\,|n_\xi\rangle\,, \tag{10}$$

where

$$|n_\xi\rangle \triangleq \frac{1}{\sqrt{n!}}(\hat{\mathbf{B}}^\dagger(\xi)^\dagger)^n\,|0\rangle \tag{11}$$

is a continuous-mode number state. (10) is similar to Eq. (4.3.1) in [30], with the exception of replacing the bosonic single-mode annihilation operator $\hat{a}$ with the continuous-mode operator $\hat{\mathbf{B}}(\xi)$ and accordingly $|n\rangle$ with $|n_\xi\rangle$.

It is easy to show that the continuous-mode single-photon coherent state $|\alpha_\xi\rangle$ is the eigenstate of $\hat{\mathbf{B}}(\xi)$, that is

$$\hat{\mathbf{B}}(\xi)\,|\alpha_\xi\rangle = \alpha\,|\alpha_\xi\rangle\,. \tag{12}$$

Moreover,

$$\left\langle\alpha_\xi|\hat{\mathbf{B}}(\xi)|\alpha_\xi\right\rangle = \left\langle\alpha_\xi|\hat{\mathbf{B}}^\dagger(\xi)|\alpha_\xi\right\rangle = \alpha\,\langle\alpha_\xi|\alpha_\xi\rangle = \alpha. \tag{13}$$

And the mean photon number is

$$\left\langle\alpha_\xi|\hat{\mathbf{B}}^\dagger(\xi)\hat{\mathbf{B}}(\xi)|\alpha_\xi\right\rangle = |\alpha|^2 = 1. \tag{14}$$

This is the reason why $|\alpha_\xi\rangle$ is a *single-photon* coherent state.

Notice that for any function $\mu[\omega]$,

$$\mathbb{E}_{\alpha_\xi}\left[e^{i\int_{-\infty}^{\infty}d\omega\;\mu[\omega]\hat{b}^\dagger[\omega]+\mu^*[\omega]\hat{b}[\omega]}\right] = \exp\left[-\frac{1}{2}\|\mu\|^2 + i\left(\langle\eta^*|\mu\rangle + \langle\eta|\mu^*\rangle\right)\right], \tag{15}$$

where $\eta \triangleq \alpha\xi$ and the subscript "α_ξ" indicates that the expectation is taken with respect to $|\alpha_\xi\rangle$. Thus, by the characteristic function theory, $|\alpha_\xi\rangle$ is a Gaussian state. More discussions on continuous-mode coherent states can be found in, e.g., [13, Eq. (3.1)], [35], and [24, Section II.E]. It should be emphasized that the Mandel's Q parameters for single-photon Fock state and coherent state are different. The Mandel's Q parameter for Fock state is less than 0, which indicates the sub-Poissonian statistics. While coherent states have a Poissonian photon-number statistics for which $Q = 0$.

Remark 1 *In fact, for the continuous-mode single-photon coherent state, $\alpha\xi[\omega] = e^{i\theta}\xi[\omega]$ plays the same role as $\alpha(\omega)$ in [13, Eq. (3.1)]. For the continuous-mode single-photon state $|1_\xi\rangle$, (3) is also defined in Section III-B in [13, Eq. (3.1)]. See also [36, Eq. (3)], [3, Chapter 6], [31, Eq. (9)], [37, Chapter 5], [15, Eq. (19)], [20, Eq. (17)], [24, Eq. (34)].*

2.2. Wigner distribution function and Wigner spectrum

Due to the singular commutation relations (1) and (5), for the continuous-mode single-photon Fock state $|1_\xi\rangle$, we have

$$\Big\langle 1_\xi|\hat{b}(t)\hat{b}^\dagger(\tau)|1_\xi\Big\rangle = \delta(t-\tau) + \xi(t)\xi^*(\tau). \tag{16}$$

(16) shows the non-stationarity of the single-photon state $|1_\xi\rangle$. The presence of the Dirac delta function is cumbersome for the statistical analysis of the single-photon state $|1_\xi\rangle$. So *normal ordering* is often used. For example, the normal ordering of $\hat{b}(t)\hat{b}^\dagger(r)$ is

$$: \hat{b}(t)\hat{b}^\dagger(\tau) := \hat{b}^\dagger(\tau)\hat{b}(t). \tag{17}$$

Notice that in this case,

$$\Big\langle 1_\xi| : \hat{b}(t)\hat{b}^\dagger(\tau) : |1_\xi\Big\rangle = \xi(t)\xi^*(\tau). \tag{18}$$

That is, the Dirac delta function is removed. Because of this, time ordering is commonly used in quantum optics, see e.g., [30]. In this paper, we adopt an alternative method for analyzing the statistical properties of input and output quantum signals. The method we use belongs to the time-frequency analysis. Let $x(t)$ be a quantum variable, see, e.g., $\hat{b}(t)$, $\hat{b}^\dagger(t)$ or $\hat{b}(t)\hat{b}^\dagger(t)$, define the two-time autocorrelation function

$$r_x(t,\tau) \triangleq \mathbb{E}_\xi[x(t)x^\dagger(\tau)], \tag{19}$$

where the subscript "ξ" indicates that the expectation is taken with respect to the single-photon state $|1_\xi\rangle$. Clearly, by (16) we have

$$r_{\hat{b}}(t,\tau) = \mathbb{E}_\xi[\hat{b}(t)\hat{b}^\dagger(\tau)] = \delta(t-\tau) + \xi(t)\xi^*(\tau). \tag{20}$$

Similarly, by normal ordering,

$$r_{\hat{b}^\dagger}(\tau,t) = \mathbb{E}_\xi[\hat{b}^\dagger(\tau)\hat{b}(t)] = \xi(t)\xi^*(\tau) = \mathbb{E}_\xi[: \hat{b}(t)\hat{b}^\dagger(\tau) :]. \tag{21}$$

Applying the Fourier transform to the two-time autocorrelation function $r_x(t,\tau)$ with respect to the time variable τ, yields

$$S_x(t,\omega) = \frac{1}{\sqrt{2\pi}}\int_{-\infty}^{\infty} r_x(t,\tau)e^{-i\omega\tau}d\tau. \tag{22}$$

Define

$$W_x(t,\omega) \triangleq \frac{1}{\sqrt{2\pi}} \int_{-\infty}^{\infty} x(t)x^\dagger(\tau)e^{-i\omega\tau}d\tau. \tag{23}$$

Clearly, by (19), (22), and (23) we have

$$S_x(t,\omega) = \mathbb{E}_\xi \left[W_x(t,\omega)\right]. \tag{24}$$

In the literature, $W_x(t,\omega)$ is called the *Wigner-Ville distribution function,* or simply *Wigner function*, and accordingly $S_x(t,\omega)$ the *Wigner spectrum*, [26], [38], [39]. Notice that

$$S_{\hat{b}}(t,\omega) = \frac{1}{\sqrt{2\pi}} e^{-i\omega t} + \xi(t)\xi^*[\omega]. \tag{25}$$

Comparing (20) and (25), we see that the Dirac delta function does not appear in the Wigner spectrum $S_x(t,\omega)$. Motivated by this, in this paper we use Wigner spectrum to analyze the statistical properties of quantum signals, instead of resorting to normal ordering.

2.3. Optical cavity

Briefly speaking, an optical cavity G consists of two mirrors which are aligned on one optical axis such that the incident light can be reflected in a closed path [40, Chapter 7.1], [41, Chapter 5.3]. The dynamics of the intracavity field operator $\hat{a}(t)$ can be described with the following quantum stochastic differential equations

$$\dot{\hat{a}}(t) \quad = (-\frac{\kappa}{2} - i\omega_0)\hat{a}(t) - \sqrt{\kappa}\hat{b}_{\rm in}(t), \tag{26a}$$

$$\hat{b}_{\rm out}(t) = \sqrt{\kappa}\hat{a}(t) + \hat{b}_{\rm in}(t), \tag{26b}$$

where $[\hat{a}, \hat{a}^\dagger] = 1$, $\hat{b}_{\rm in}(t)$ ($\hat{b}_{\rm out}(t)$) is the input (output) field which satisfies $[\hat{b}(t_1), \hat{b}^\dagger(t_2)] = \delta(t_1 - t_2)$, κ is the cavity decay rate and ω_0 is the de-tuning. The impulse response function for this system G is given by

$$g_G(t) = \delta(t) - \kappa e^{(-\frac{\kappa}{2} - i\omega_0)t}, \quad t \geq 0, \tag{27}$$

while $g_G(t) \equiv 0$ when $t < 0$. Let $|1_\nu\rangle$ be a continuous-mode single-photon state

$$|1_\nu\rangle \equiv \mathbf{B}^\dagger(\nu)|0\rangle := \int_{-\infty}^{\infty} b_{\rm in}^\dagger(t)\nu(t)dt|0\rangle \tag{28}$$

with pulse shape

$$\nu(t) = \begin{cases} \sqrt{2\gamma}e^{-\gamma t}, & t \geq 0, \\ 0, & t < 0. \end{cases} \tag{29}$$

The state $|1_\nu\rangle$ can describe a single-photon field emitted from an optical cavity with damping rate $\sqrt{2\gamma}$ [3, 40]. Then the input covariance function is

$$R_{\rm in}(t,r) = \begin{bmatrix} \delta(t-r) & 0 \\ 0 & 0 \end{bmatrix} + \begin{bmatrix} \nu^*(r)\nu(t) & 0 \\ 0 & \nu^*(t)\nu(r) \end{bmatrix}. \tag{30}$$

On the other hand, by the input-output relation [24], the steady-state output single-photon state $|1_\eta\rangle$ has the pulse shape

$$\eta(t) = \sqrt{2\gamma}e^{-\gamma t} - \frac{\kappa\sqrt{2\gamma}}{\frac{\kappa}{2} + i\omega_0 - \gamma}\left(e^{-\gamma t} - e^{(-\frac{\kappa}{2} - i\omega_0)t}\right). \tag{31}$$

Write

$$\chi(t, r) = \delta(t - r), \tag{32}$$

then the steady-state output covariance function is

$$R_{\text{out}}(t, r) = \chi(t, r)\begin{bmatrix} 1 & 0 \\ 0 & 0 \end{bmatrix} + \begin{bmatrix} \eta(t)\eta^*(r) & 0 \\ 0 & \eta^*(t)\eta(r) \end{bmatrix}. \tag{33}$$

By (22) and (30), the Wigner spectrum of the input covariance function can be expressed in terms of both time and frequency

$$S_{\text{in}}(t, \omega) = \frac{1}{\sqrt{2\pi}}\begin{bmatrix} e^{-i\omega t} & 0 \\ 0 & 0 \end{bmatrix} + \frac{1}{\sqrt{2\pi}}\begin{bmatrix} \frac{2\gamma}{\gamma + i\omega}e^{-\gamma t} & 0 \\ 0 & \frac{2\gamma}{\gamma + i\omega}e^{-\gamma t} \end{bmatrix}. \tag{34}$$

Similarly, by (22) and (33), we can get the Wigner spectrum of the output covariance function

$$S_{\text{out}}(t, \omega) = \frac{1}{\sqrt{2\pi}}\begin{bmatrix} e^{-i\omega t} & 0 \\ 0 & 0 \end{bmatrix} + \frac{1}{\sqrt{2\pi}}\begin{bmatrix} \eta(t)S_{11}(\omega) & 0 \\ 0 & \eta^*(t)S_{22}(\omega) \end{bmatrix}, \tag{35}$$

where

$$S_{11}[\omega] = \sqrt{2\gamma} \times \frac{-\frac{1}{4}\kappa^2 + \frac{1}{2}\kappa\gamma - \omega_0^2 + \omega\omega_0 + i[\gamma\omega_0 + \frac{1}{2}\omega\kappa - \omega\gamma]}{(\gamma + i\omega)(\frac{\kappa}{2} - i\omega_0 - \gamma)(\frac{\kappa}{2} - i\omega_0 + i\omega)}, \tag{36a}$$

$$S_{22}[\omega] = \sqrt{2\gamma} \times \frac{-\frac{1}{4}\kappa^2 + \frac{1}{2}\kappa\gamma - \omega_0^2 - \omega\omega_0 + i[-\gamma\omega_0 + \frac{1}{2}\omega\kappa - \omega\gamma]}{(\gamma + i\omega)(\frac{\kappa}{2} + i\omega_0 - \gamma)(\frac{\kappa}{2} + i\omega_0 + i\omega)}. \tag{36b}$$

If we let decay rate $\kappa \to \infty$, then the following equation holds

$$S_{\text{out}}(t, \omega) = S_{\text{in}}(t, \omega). \tag{37}$$

That is, the output single-photon state is identical to the input single-photon state.

It should be noted that the quantities plotted are dimensionless throughout the paper. In the following we fix damping rate $\gamma = 2$. In Fig. 1, (a) and (b) are the diagonal entries of the input Wigner spectrum respectively and both of them are exponentially decaying with respect to time t. Fig. 2, Fig. 3 and Fig. 4 are the output Wigner spectra with different decay rates κ and the same de-tuning $\omega_0 = 0$. Fig. 5, Fig. 6 and Fig. 7 are the output Wigner spectra with same decay rate $\kappa = 4$ and different de-tunings ω_0.

By comparing these figures, we can see that there exist five cases. **Case 1**: the output Wigner spectrum will be close to the input when the decay rate κ is very small and this can be explained by comparing (34) and (35) directly. **Case 2**: the output Wigner spectrum will also be close to the input when the decay rate κ is very large. Since the impulse response function $g_G(t) \to \delta(t)$ when $\kappa \to \infty$, then the output state will be close to the input state. **Case 3**: the output Wigner spectrum would be much

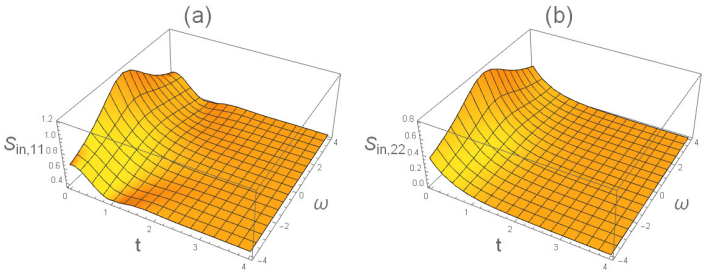

Figure 1. (Color online) (a) and (b) are the diagonal entries of the input Wigner spectrum.

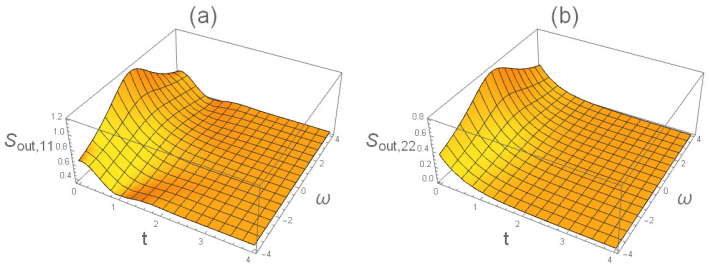

Figure 2. (Color online) (a) and (b) are the diagonal entries of the output Wigner spectrum with de-tuning $\omega_0 = 0$ and decay rate $\kappa = 0$. The output Wigner spectrum is as same as the input since the output covariance function reduces to the input.

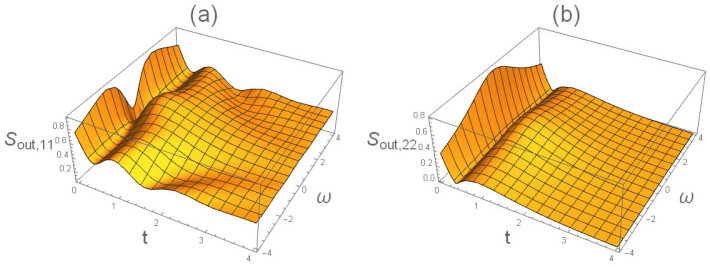

Figure 3. (Color online) (a) and (b) are the diagonal entries of the output Wigner spectrum with de-tuning $\omega_0 = 0$ and decay rate $\kappa = 3$. Compared with the input, output Wigner spectrum is no longer monotonic in $\omega = 0$ since decay rate κ becomes larger.

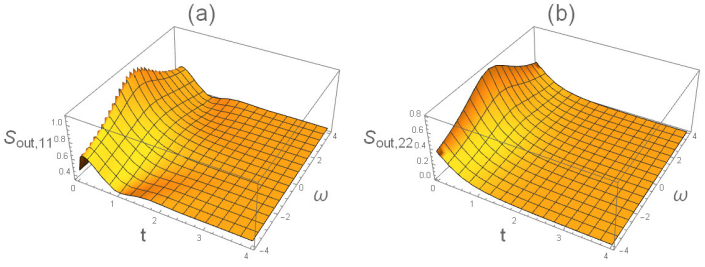

Figure 4. (Color online) (a) and (b) are the diagonal entries of the output Wigner spectrum with de-tuning $\omega_0 = 0$ and decay rate $\kappa = 100$. The output Wigner spectrum is much similar to the input when decay rate κ is large.

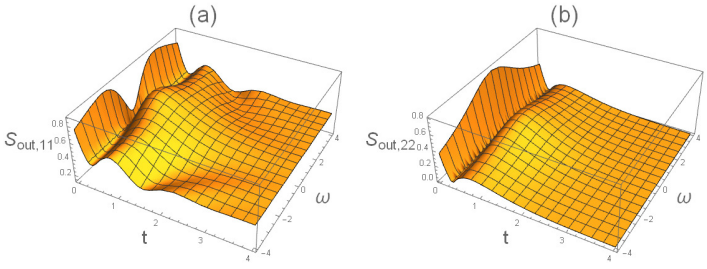

Figure 5. (Color online) (a) and (b) are the diagonal entries of the output Wigner spectrum with decay rate $\kappa = 4$ and de-tuning $\omega_0 = 0$. In contrast to the decay rate κ, the output Wigner spectrum is much unlike the input even de-tuning ω_0 is very small.

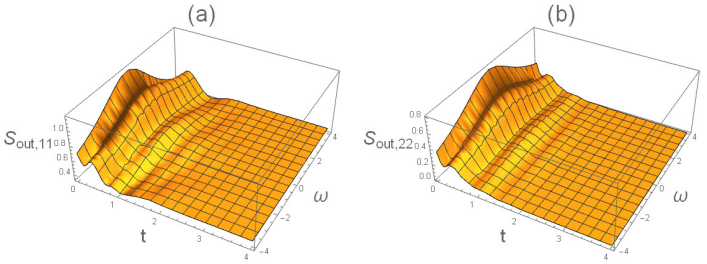

Figure 6. (Color online) (a) and (b) are the diagonal entries of the output Wigner spectrum with decay rate $\kappa = 4$ and de-tuning $\omega_0 = 10$. When de-tuning ω_0 becomes larger, the output Wigner spectrum will tend to be the input.

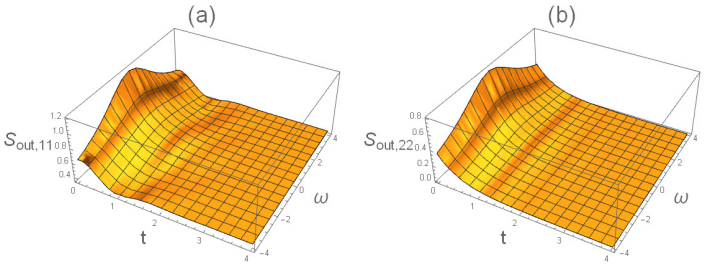

Figure 7. (Color online) (a) and (b) are the diagonal entries of the output Wigner spectrum with decay rate $\kappa = 4$ and de-tuning $\omega_0 = 50$. Finally, if de-tuning ω_0 is sufficiently large, the output Wigner spectrum would be close to the input.

similar to the input when the de-tuning ω_0 is very large since the optical cavity has little influence on the photons, see Fig. 7. **Case 4**: it can be seen from Fig. 3 that the output Wigner spectrum is quite different from the input one when κ is not very large or small. Moreover, (a) (for $\hat{b}_{\text{out}}\hat{b}^{\dagger}_{\text{out}}$) and (b) (for $\hat{b}^{\dagger}_{\text{out}}\hat{b}_{\text{out}}$) are quite different. **Case 5**: The output Wigner spectrum would change a lot with a small de-tuning since there exists a strong interaction between the photon and system (compare Figs. 1 and 5). Therefore, with Wigner spectrum, we are able to observe the changes of the system's response to the input signals in time and frequency domain simultaneously. This has not been done before in the single-photon setting.

3. Wigner spectrum for degenerate parametric amplifier

A degenerate parametric amplifier (DPA) is an open oscillator that is able to produce squeezed output fields [30, Chapter 6.3], [40, Chapter 7.6], [41, Chapter 6.3].

A model for a DPA is [24]

$$\begin{bmatrix} \dot{\hat{a}}(t) \\ \dot{\hat{a}}^\dagger(t) \end{bmatrix} = -\frac{1}{2}\begin{bmatrix} \kappa & -\epsilon \\ -\epsilon & \kappa \end{bmatrix}\begin{bmatrix} \hat{a}(t) \\ \hat{a}^\dagger(t) \end{bmatrix} - \sqrt{\kappa}\begin{bmatrix} \hat{b}_{\rm in}(t) \\ \hat{b}_{\rm in}^\dagger(t) \end{bmatrix}, \tag{38a}$$

$$\hat{b}_{\rm out}(t) = \sqrt{\kappa}\hat{a}(t) + \hat{b}_{\rm in}(t), \quad (0 < \epsilon < \kappa). \tag{38b}$$

The steady output state is no longer a single-photon state because the DPA has pump and the system is not passive any more. The steady output state belongs to the class of photon-Gaussian states which is defined in [24]. Here we assume that the single-photon input state $|1_\nu\rangle$ is that defined in (29), then the output covariance function is

$$R_{\rm out}(t,r) = \begin{bmatrix} \chi_{11}(t,r) & \chi_{12}(t,r) \\ \chi_{21}(t,r) & \chi_{22}(t,r) \end{bmatrix} + \Delta(\xi_{\rm out}^-(t), \xi_{\rm out}^+(t))\Delta(\xi_{\rm out}^-(r), \xi_{\rm out}^+(r))^\dagger, \tag{39}$$

and the Wigner spectrum of output covariance function for the DPA is

$$S_{\rm out}(t,\omega) = \begin{bmatrix} S_{{\rm out},11}(t,\omega) & S_{{\rm out},12}(t,\omega) \\ S_{{\rm out},21}(t,\omega) & S_{{\rm out},22}(t,\omega) \end{bmatrix}. \tag{40}$$

Here, the explicit forms of output covariance function $R_{\rm out}(t,r)$ and Wigner spectrum $S_{\rm out}(t,\omega)$ are given in Appendix Appendix A. Similar with the cavity case, if we let decay rate $\kappa \to \infty$, (37) also holds for the DPA case, which is consistent with the simulation result in Fig. 10.

In the following we fix $\epsilon = 1$, $\gamma = 2$. The input Wigner spectrum is as same as the optical cavity case in Fig. 1. In Fig. 8, $S_{{\rm out},11}(t,\omega)$, $S_{{\rm out},12}(t,\omega)$, $S_{{\rm out},21}(t,\omega)$, $S_{{\rm out},22}(t,\omega)$ are the entries for the output Wigner spectrum in (40) respectively, as same as in Fig. 9 and Fig. 10. Those are the Wigner spectra for the DPA case with different decay rates κ. Compared with the cavity case, there exists non-zero off-diagonal parts since DPA is a non-passive system. Moreover, it can be seen clearly from Figs. 8 and 9 that the photon-Gaussian state is significantly different from the single-photon state. A photon-Gaussian state is obtained by driving a DPA with a single-photon state, [24]. Intuitively, a photon-Gaussian state is of the form $\mathbf{B}^\dagger(\eta)|\alpha\rangle$ in which η is a pulse shape and $|\alpha\rangle$ is a coherent state. Clearly, when $|\alpha\rangle = |0\rangle$, we get a single-photon state.

Now we have considered the Wigner spectra for optical cavity and DPA. And we can see that the output Wigner spectrum will be much similar with the input when the decay rates are larger. In the DPA case, since the active system must be stable, we need decay rate κ to be greater than ϵ. But if we let ϵ be a very small parameter, then decay rate κ can go to 0. By the explicit form of output Wigner spectrum in Appendix A, we can prove that the output Wigner spectrum would be similar with the input, as same as the optical cavity case. And all the trends can be verified by the explicit forms of the input and output Wigner spectrum mathematically.

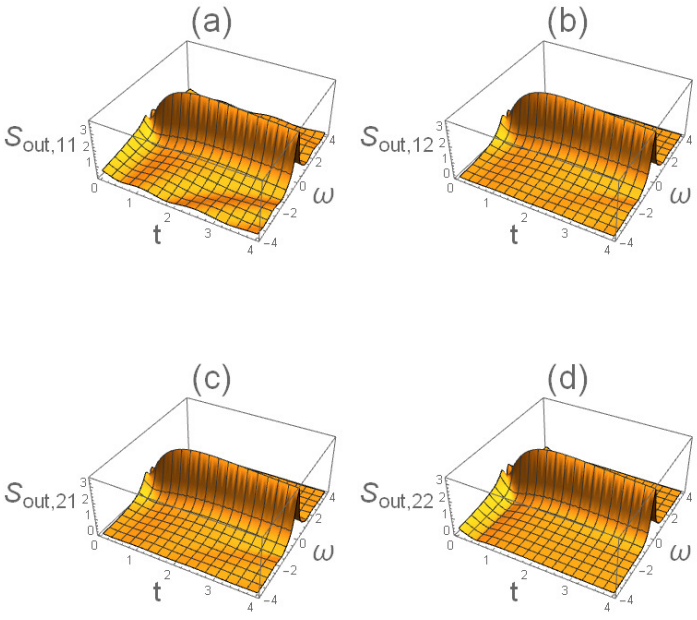

Figure 8. (Color online) The output Wigner spectrum with $\epsilon = 1$, $\gamma = 2$ and decay rate $\kappa = 1.5$. Compared with the passive system (optical cavity), the off-diagonal entries are non-zero and this output Wigner spectrum is much different since DPA is an active system. And the decay rate κ must be greater than ϵ to make the system stable.

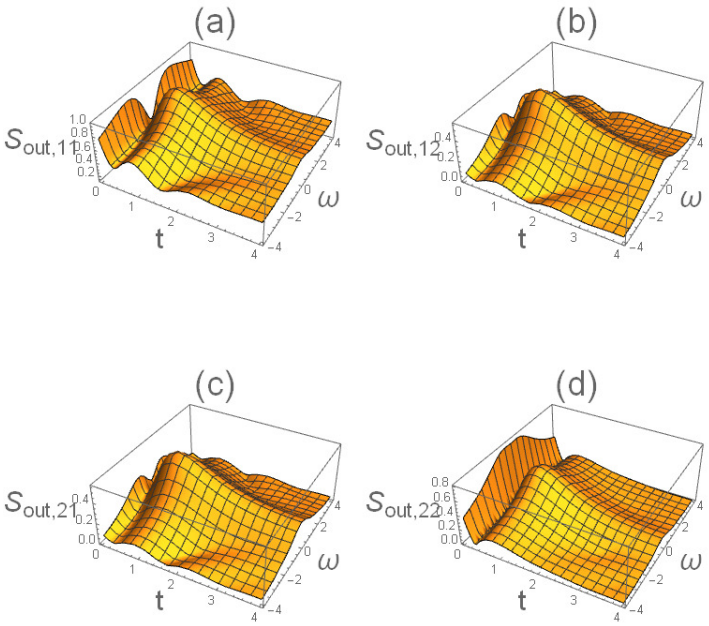

Figure 9. (Color online) The output Wigner spectrum with $\epsilon = 1$, $\gamma = 2$ and decay rate $\kappa = 4$. The output Wigner spectrum becomes non-monotonic with a larger decay rate κ. Compared with Fig. 4, it can be seen that the 1-by-1 and 2-by-2 entries converge to 0 more slowly with same decay rate $\kappa = 4$. What's more, the off-diagonal entries cannot be ignored since the corresponding amplitudes are close to 0.4.

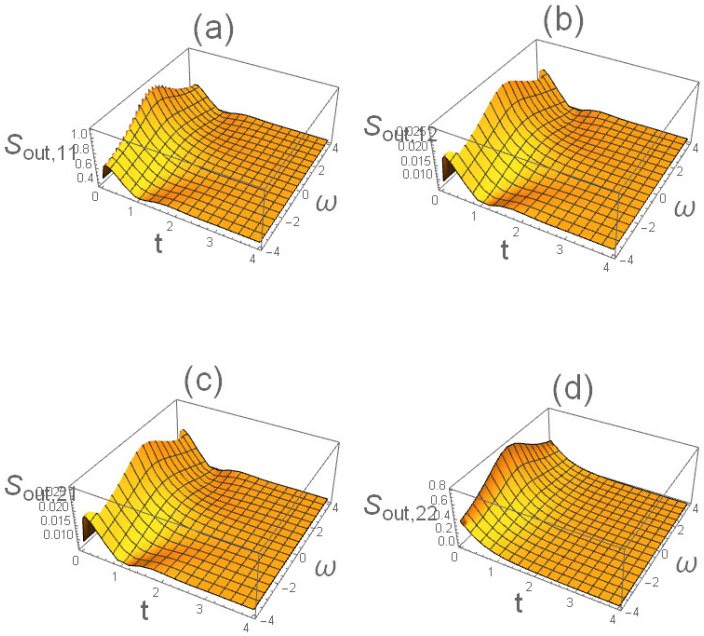

Figure 10. (Color online) The output Wigner spectrum with $\epsilon = 1$, $\gamma = 2$ and decay rate $\kappa = 100$. If we compare the four parts in one figure, it can be seen that the amplitudes in 1-by-2 and 2-by-1 entries are almost 0 (the corresponding amplitudes are less than 0.025). Thus, the output Wigner spectrum would be similar with the input when decay rate κ is large enough although DPA is non-passive.

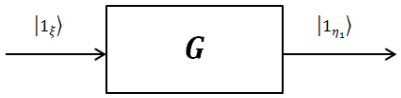

Figure 11. The original system G.

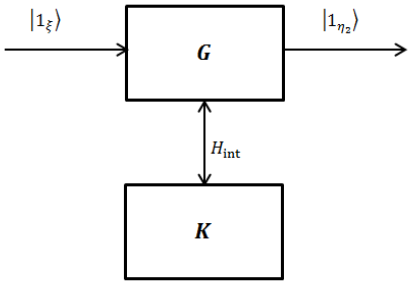

Figure 12. Directly coupled system $G \bowtie K$.

4. Photon pulse shape engineering

In this section, we will discuss how to engineer photon pulse shapes by means of coherent control methods, namely direct coupling (Fig. 12) and coherent feedback (Fig. 13).

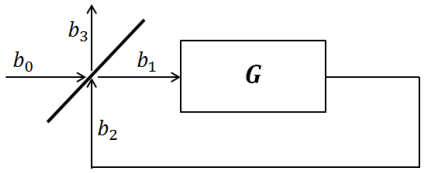

Figure 13. Linear quantum feedback network consisting of a beamsplitter.

4.1. Direct couplings

In Fig. 12, two independent systems G and K may interact by exchanging energy. This energy exchange can be described by an interaction Hamiltonian H_{int} with the form

$$H_{\text{int}} = X_1^\dagger X_2 + X_1 X_2^\dagger, \tag{41}$$

where X_1 and X_2 are vectors of operators on system G and K respectively. We can denote the directly coupled system by $G \bowtie K$, see [42, 43].

Quantum markovian systems can be conveniently described by the triple (S, L, H) language, in which S is the scattering operator matrix, L is the coupling between system and field, and H denotes the Hamiltonian, see [44, 45, 46].

Fig. 11 is an optical cavity with the following parameters,

$$G = (1, \sqrt{\kappa}\hat{a}_1, \omega_1 \hat{a}_1^\dagger \hat{a}_1), \tag{42}$$

where κ is the system decay rate and ω_1 denotes the de-tuning for system G. $|1_\xi\rangle$ is the single photon input state and $|1_{\eta_1}\rangle$ is the output state. In Fig. 12, the system G is directly coupled with another quantum system K with parameters

$$K = (-, -, \omega_2 \hat{a}_2^\dagger \hat{a}_2), \tag{43}$$

where ω_2 denotes the de-tuning for system K. In this case, the output state is described by $|1_{\eta_2}\rangle$. Alternatively, we may use a beamsplitter to form a coherent feedback system, see Fig. 13. In the following, we will derive the explicit forms of output pulse shapes in the frequency domain.

4.2. Photon shape synthesis

Let the pulse shape of a single-photon input state $|1_\xi\rangle$ be

$$\xi(t) = \begin{cases} \sqrt{2\beta} e^{-\beta t}, & t \geq 0, \\ 0, & t < 0, \end{cases} \tag{44}$$

where β is the damping rate. By Fourier transform, we can get the input pulse shape in the frequency domain

$$\xi[\omega] = \frac{\sqrt{2\beta}}{i\omega + \beta}. \tag{45}$$

The transfer function for the original system G is given by

$$G_1[\omega] = 1 - \frac{\kappa}{i\omega + i\omega_1 + \frac{\kappa}{2}}, \tag{46}$$

and the output pulse shape in the frequency domain is

$$\eta_1[\omega] = \left(1 - \frac{\kappa}{i\omega + i\omega_1 + \frac{\kappa}{2}}\right)\xi[\omega]. \tag{47}$$

Secondly, for the directly coupled system in Fig. 12, we assume that $X_1 = \alpha\hat{a}_1$, $\alpha \in \mathbb{C}$ and $X_2 = \hat{a}_2$. The interaction Hamiltonian is given by

$$H_{\text{int}} = \bar{\alpha}\hat{a}_1^\dagger\hat{a}_2 + \alpha\hat{a}_1\hat{a}_2^\dagger. \tag{48}$$

Then the Hamiltonian for the whole system $G \bowtie K$ is

$$H = H_1 + H_{\text{int}} + H_2, \tag{49}$$

where $H_1 = \omega_1\hat{a}_1^\dagger\hat{a}_1$, $H_2 = \omega_2\hat{a}_2^\dagger\hat{a}_2$.

We get the output pulse shape for the system $G \bowtie K$, which is

$$\eta_2[\omega] = \frac{-\frac{\kappa}{2}(\omega+\omega_2)i - (\omega+\omega_1)(\omega+\omega_2) + |\alpha|^2}{\frac{\kappa}{2}(\omega+\omega_2)i - (\omega+\omega_1)(\omega+\omega_2) + |\alpha|^2}\xi[\omega]. \tag{50}$$

Finally, in Fig. 13, let the beamsplitter be

$$S = \begin{bmatrix} \sqrt{\gamma} & e^{-i\phi}\sqrt{1-\gamma} \\ -e^{i\phi}\sqrt{1-\gamma} & \sqrt{\gamma} \end{bmatrix}, 0 < \gamma < 1, \tag{51}$$

and b_0 be in the single-photon state $|1_\xi\rangle$. We can get the pulse shape for the output field b_3 in Fig. 13

$$\eta_3[\omega] = \frac{-\frac{1-\sqrt{\gamma}}{1+\sqrt{\gamma}}(\omega+\omega_1)i + \frac{\kappa}{2}}{\frac{1-\sqrt{\gamma}}{1+\sqrt{\gamma}}(\omega+\omega_1)i + \frac{\kappa}{2}}\xi[\omega]. \tag{52}$$

4.3. Photon distribution

For the single photon state we defined before

$$|1_\xi\rangle = \int_{-\infty}^{\infty} \hat{b}_{\text{in}}^\dagger(t)\xi(t)dt|0\rangle, \tag{53}$$

$\hat{b}_{\text{in}}^\dagger(t)$ is the creation operator and $\xi(t)$ is the pulse shape which is also known as temporal wave packet. $|\xi(t)|^2$ denotes the probability of finding the photon (detection probability) in the interval $[t, t+dt)$. In this subsection, we will focus on how the system parameters change the detection probabilities in the control schemes discussed above.

By Inverse Fourier transform, we can get the output temporal wave packets

$$\eta_j(t) = \frac{1}{\sqrt{2\pi}}\int_{-\infty}^{\infty} e^{i\omega t}\eta_j[\omega]d\omega, \quad (j = 1, 2, 3) \tag{54}$$

where j denotes the j-th case we discussed before.

For the direct coupling scheme, Fig. 12, we fix $\beta = 2$, $\kappa = 1$, $\omega_1 = 1$. Fig. 14 and Fig. 15 are the detection probabilities for different α and ω_2 respectively. For the

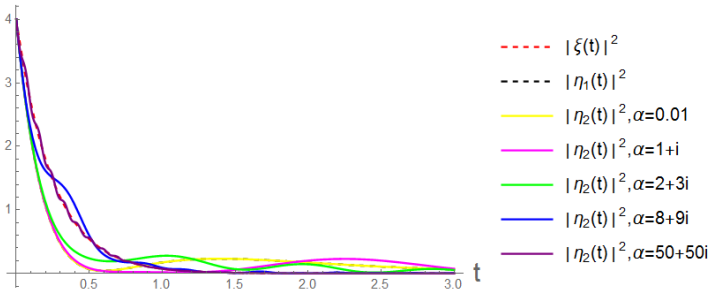

Figure 14. (Color online) $|\xi(t)|^2$ denotes the detection probability of input pulse shape, $|\eta_1(t)|^2$ denotes the detection probability of output pulse shape in the case of original system (Fig. 11), $|\eta_2(t)|^2$ are the detection probabilities of output pulse shape in the directly coupled system (Fig. 12) with different parameters α.

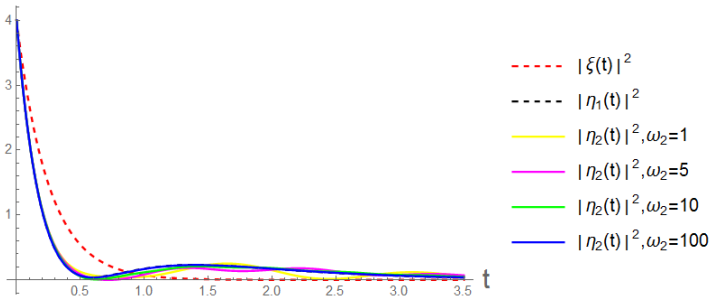

Figure 15. (Color online) $|\xi(t)|^2$ denotes the detection probability of input pulse shape, $|\eta_1(t)|^2$ denotes the detection probability of output pulse shape in the case of original system (Fig. 11), $|\eta_2(t)|^2$ are the detection probabilities of output pulse shape in the directly coupled system (Fig. 12) with different parameters ω_2.

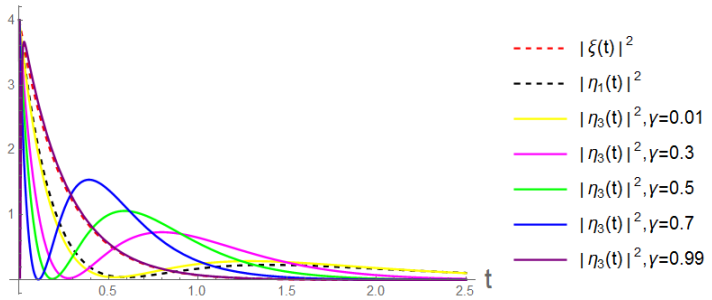

Figure 16. (Color online) $|\xi(t)|^2$ denotes the detection probability of input pulse shape, $|\eta_1(t)|^2$ denotes the detection probability of output pulse shape in the case of original system (Fig. 11), $|\eta_3(t)|^2$ are the detection probabilities of output pulse shape in the linear quantum feedback network (Fig. 13) with different beamsplitter parameters γ.

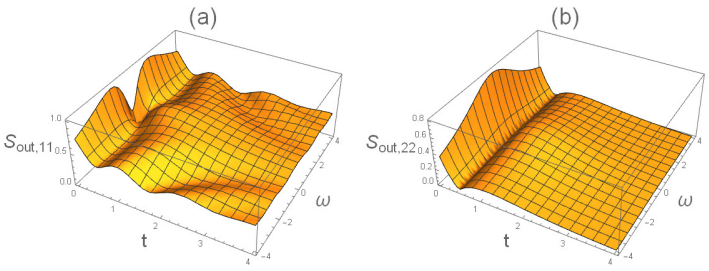

Figure 17. (Color online) The output Wigner spectrum for quantum feedback network with beamsplitter parameter $\gamma = 0.01$. Since $b_3 \to b_2$, $b_1 \to b_0$ when $\gamma \to 0$, the feedback network should reduce to the original system without beamsplitter. This can be verified by comparison with Fig. 3.

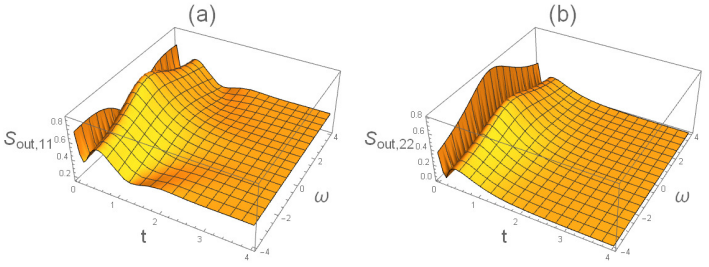

Figure 18. (Color online) The output Wigner spectrum for quantum feedback network with beamsplitter parameter $\gamma = 0.5$.

coherent feedback control case Fig. 13, detection probabilities for different beamsplitter parameter γ are given in Fig. 16.

By comparing these three cases, it can be easily seen that the linear quantum feedback network in Fig. 13 has much more influence on the detection probability than the directly coupled system. In addition, the changes of output Wigner spectrum with beamsplitter parameter γ for quantum feedback network also have been analyzed. In Fig. 17 - Fig. 19, let the decay rate of the optical cavity be $\kappa = 4$ and damping rate be $\beta = 2$, it can be verified that those changes are consistent with the photon distributions in Fig. 16.

On the other hand, we assume the system G for the feedback network in Fig. 13 is a DPA with the triple (S, L, H) parameters

$$S_0 = I, \quad L_0 = \sqrt{\kappa}\hat{a}, \quad H_0 = \frac{i\epsilon}{4}((\hat{a}^\dagger)^2 - \hat{a}^2). \tag{55}$$

Then the whole feedback network system parameters with beamsplitter S are given by

$$S_1 = -I, \quad L_1 = \sqrt{\frac{1+\sqrt{\gamma}}{1-\sqrt{\gamma}}}\kappa\hat{a}, \quad H_1 = H_0. \tag{56}$$

So the only change between the feedback network and the original system is $\kappa \to \frac{1+\sqrt{\gamma}}{1-\sqrt{\gamma}}\kappa$. There exist three cases as follows:

1) $\gamma = 0$, the feedback network reduces to the open-loop system G.

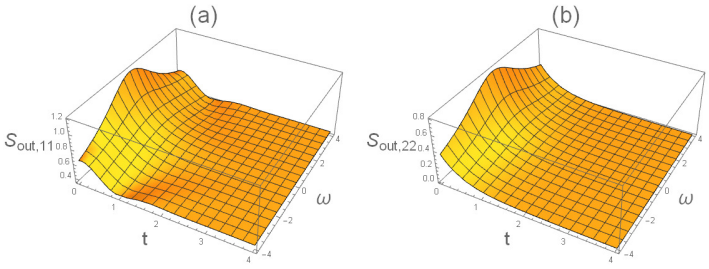

Figure 19. (Color online) The output Wigner spectrum for quantum feedback network with beamsplitter parameter $\gamma = 0.99$. If $\gamma \to 1$, then $b_3 \to b_0$. It means that the output Wigner spectrum will be close to the input. Thus, the simulation result should be much similar with the input Wigner spectrum in Fig. 1.

2) $\gamma = 1$, then $S = I$, $b_3 = b_0$, there is no interaction between field and system.
3) $0 < \gamma < 1$, $\frac{1+\sqrt{\gamma}}{1-\sqrt{\gamma}}\kappa > \kappa$, the decay rate is always enhanced. However, it is clear that

$$\lim_{\gamma \to 0} \frac{1+\sqrt{\gamma}}{1-\sqrt{\gamma}}\kappa = \kappa. \tag{57}$$

Therefore, by tuning the beamsplitter we can get various output single-photon states. It is worth noting that the same feedback scheme Fig. 13 has been used for optical squeezing, see theoretical [47] and experimental [48].

5. Conclusion

In this article, Wigner distribution and Wigner spectrum have been used to analyze the response of quantum linear systems to single-photon input states. In contrast to normal ordering, they are able to provide full information of the quantum states, in time and frequency domains simultaneously. Several control schemes are compared for photon pulse shaping. It has been demonstrated that the coherent feedback control scheme is very effective in photon pulse shaping.

References

[1] Beveratos A, Brouri R, Gacoin T, Villing A, Poizat J P and Grangier P 2002 *Physical Review Letters* **89** 187901

[2] Gisin N and Thew R 2007 *Nature photonics* **1** 165–171

[3] Loudon R 2000 *The quantum theory of light* (Oxford university press)

[4] Knill E, Laflamme R and Milburn G J 2001 *nature* **409** 46–52

[5] Giovannetti V, Lloyd S and Maccone L 2004 *Science* **306** 1330–1336

[6] Giovannetti V, Lloyd S and Maccone L 2011 *Nature Photonics* **5** 222

[7] Leroux I D, Schleier-Smith M H, Zhang H and Vuletić V 2012 *Physical Review A* **85** 013803

[8] Kimble H J 2008 *Nature* **453** 1023

[9] Moehring D, Maunz P, Olmschenk S, Younge K, Matsukevich D, Duan L M and Monroe C 2007 *Nature* **449** 68

[10] Aghamalyan D and Malakyan Y 2011 *Physical Review A* **84** 042305

[11] Furusawa A and Van Loock P 2011 *Quantum teleportation and entanglement: a hybrid approach to optical quantum information processing* (John Wiley & Sons)

[12] Braunstein S L and Van Loock P 2005 *Reviews of Modern Physics* **77** 513

[13] Blow K, Loudon R, Phoenix S J and Shepherd T 1990 *Physical Review A* **42** 4102

[14] Brecht B, Reddy D V, Silberhorn C and Raymer M G 2015 *Physical Review X* **5** 041017

[15] Wang Y, Minář J, Sheridan L and Scarani V 2011 *Physical Review A* **83** 063842

[16] Baragiola B Q, Cook R L, Brańczyk A M and Combes J 2012 *Physical Review A* **86** 013811

[17] Ogawa H, Ohdan H, Miyata K, Taguchi M, Makino K, Yonezawa H, Yoshikawa J i and Furusawa A 2016 *Physical Review Letters* **116** 233602

[18] Gough J E, James M R and Nurdin H I 2011 *50th IEEE Conference on Decision and Control and European Control Conference* 5570–5576

[19] Gough J E, James M R and Nurdin H I 2013 *Quantum information processing* **12** 1469

[20] Gough J E, James M R, Nurdin H I and Combes J 2012 *Physical Review A* **86** 043819

[21] Song H, Zhang G and Xi Z 2016 *SIAM Journal on Control and Optimization* **54** 1602–1632

[22] Carvalho A, Hush M and James M 2012 *Physical Review A* **86** 023806

[23] Wiseman H M and Milburn G J 2009 *Quantum measurement and control* (Cambridge University Press)

[24] Zhang G and James M R 2013 *Automatic Control, IEEE Transactions on* **58** 1221

[25] Zhang G 2014 *Automatica* **50** 442

[26] Wigner E 1932 *Physical Review* **40** 749

[27] Lvovsky A I, Hansen H, Aichele T, Benson O, Mlynek J and Schiller S 2001 *Physical Review Letters* **87** 050402

[28] Yukawa M, Miyata K, Mizuta T, Yonezawa H, Marek P, Filip R and Furusawa A 2013 *Optics express* **21** 5529

[29] Qin Z, Prasad A S, Brannan T, MacRae A, Lezama A and Lvovsky A 2015 *Light: Science & Applications* **4** e298

[30] Gardiner C and Zoller P 2004 *Quantum noise: a handbook of Markovian and non-Markovian quantum stochastic methods with applications to quantum optics* vol 56 (Springer Science & Business Media)

[31] Milburn G 2008 *The European Physical Journal Special Topics* **159** 113

[32] Barzanjeh S, Abdi M, Milburn G, Tombesi P and Vitali D 2012 *Physical review letters* **109** 130503

[33] Pan Y, Zhang G and James M R 2016 *Automatica* **69** 18–23

[34] Yamamoto N and James M R 2014 *New Journal of Physics* **16** 073032

[35] Gough J E 2005 *Russian Journal of Mathematical Physics* **10** 142–148

[36] Gheri K M, Ellinger K, Pellizari T and Zoller P 1998 *Fortschritte der Physik* **46** 401–416

[37] Garrison J and Chiao R 2008 *Quantum optics* (Oxford University Press)

[38] Ville J d *et al.* 1948 *Cables et transmission* **2** 61–74

[39] Sandsten M 2013 *Time-Frequency Analysis of Non-Stationary Processes* (Lund University, Centre for Mathematical Sciences)

[40] Walls D F and Milburn G J 2007 *Quantum optics* (Springer Science & Business Media)

[41] Bachor H A and Ralph T C 2004 *A guide to experiments in quantum optics* (Wiley)

[42] Wiseman H M and Milburn G J 1994 *Physical review A* **49** 4110

[43] Zhang G and James M R 2011 *Automatic Control, IEEE Transactions on* **56** 1535

[44] Gough J and James M R 2009 *Automatic Control, IEEE Transactions on* **54** 2530

[45] Gough J E, James M and Nurdin H 2010 *Physical Review A* **81** 023804

[46] Zhang G and James M R 2012 *Chinese Science Bulletin* **57** 2200

[47] Gough J E and Wildfeuer S 2009 *Physical Review A* **80** 042107

[48] Iida S, Yukawa M, Yonezawa H, Yamamoto N and Furusawa A 2012 *Automatic Control, IEEE Transactions on* **57** 2045

Appendix A. The explicit form of output Wigner spectrum for DPA

If the single-photon input $|1_\nu\rangle$ has the pulse shape defined in (29), we can get the pulse shape of output state

$$\xi^-_{\text{out}}(t) = \frac{(\epsilon^2+\kappa^2-4\gamma^2)\sqrt{2\gamma}}{(\kappa+\epsilon-2\gamma)(\epsilon-\kappa+2\gamma)}e^{-\gamma t} + \frac{\kappa\sqrt{2\gamma}}{\kappa+\epsilon-2\gamma}e^{(-\frac{\epsilon}{2}-\frac{\kappa}{2})t} - \frac{\kappa\sqrt{2\gamma}}{\epsilon-\kappa+2\gamma}e^{(\frac{\epsilon}{2}-\frac{\kappa}{2})t},$$

$$\xi^+_{\text{out}}(t) = \frac{2\kappa\epsilon\sqrt{2\gamma}}{(\kappa+\epsilon-2\gamma)(\epsilon-\kappa+2\gamma)}e^{-\gamma t} - \frac{\kappa\sqrt{2\gamma}}{\kappa+\epsilon-2\gamma}e^{(-\frac{\epsilon}{2}-\frac{\kappa}{2})t} - \frac{\kappa\sqrt{2\gamma}}{\epsilon-\kappa+2\gamma}e^{(\frac{\epsilon}{2}-\frac{\kappa}{2})t}.$$

Then, the output covariance function is

$$R_{\text{out}}(t,r) = \begin{bmatrix} \chi_{11}(t,r) & \chi_{12}(t,r) \\ \chi_{21}(t,r) & \chi_{22}(t,r) \end{bmatrix} + \Delta(\xi^-_{\text{out}}(t),\xi^+_{\text{out}}(t))\Delta(\xi^-_{\text{out}}(r),\xi^+_{\text{out}}(r))^\dagger,$$

where

$$\chi_{11}(t,r) = \begin{cases} \frac{-\kappa\epsilon}{4(\kappa+\epsilon)}e^{(-\frac{\epsilon}{2}-\frac{\kappa}{2})(t-r)} + \frac{\kappa\epsilon}{4(\kappa-\epsilon)}e^{(\frac{\epsilon}{2}-\frac{\kappa}{2})(t-r)}, & t > r, \\ \delta(t-r) + \frac{3\kappa\epsilon^2-2\kappa^3}{2(\kappa^2-\epsilon^2)}, & t = r, \\ \frac{-\kappa\epsilon}{4(\kappa+\epsilon)}e^{(-\frac{\epsilon}{2}-\frac{\kappa}{2})(r-t)} + \frac{\kappa\epsilon}{4(\kappa-\epsilon)}e^{(\frac{\epsilon}{2}-\frac{\kappa}{2})(r-t)}, & t < r, \end{cases} \tag{A.1}$$

$$\chi_{12}(t,r) = \begin{cases} \frac{\kappa\epsilon}{4(\kappa+\epsilon)}e^{(-\frac{\epsilon}{2}-\frac{\kappa}{2})(t-r)} + \frac{\kappa\epsilon}{4(\kappa-\epsilon)}e^{(\frac{\epsilon}{2}-\frac{\kappa}{2})(t-r)}, & t > r, \\ \frac{\kappa^2\epsilon}{2(\kappa^2-\epsilon^2)}, & t = r, \\ \frac{\kappa\epsilon}{4(\kappa+\epsilon)}e^{(-\frac{\epsilon}{2}-\frac{\kappa}{2})(r-t)} + \frac{\kappa\epsilon}{4(\kappa-\epsilon)}e^{(\frac{\epsilon}{2}-\frac{\kappa}{2})(r-t)}, & t < r, \end{cases} \tag{A.2}$$

$$\chi_{21}(t,r) = \chi_{12}(t,r), \tag{A.3}$$

$$\chi_{22}(t,r) = \begin{cases} \frac{-\kappa\epsilon}{4(\kappa+\epsilon)}e^{(-\frac{\epsilon}{2}-\frac{\kappa}{2})(t-r)} + \frac{\kappa\epsilon}{4(\kappa-\epsilon)}e^{(\frac{\epsilon}{2}-\frac{\kappa}{2})(t-r)}, & t > r, \\ \frac{\kappa\epsilon^2}{2(\kappa^2-\epsilon^2)}, & t = r, \\ \frac{-\kappa\epsilon}{4(\kappa+\epsilon)}e^{(-\frac{\epsilon}{2}-\frac{\kappa}{2})(r-t)} + \frac{\kappa\epsilon}{4(\kappa-\epsilon)}e^{(\frac{\epsilon}{2}-\frac{\kappa}{2})(r-t)}, & t < r. \end{cases} \tag{A.4}$$

Thus, the Wigner spectrum of output covariance function for the DPA is

$$S_{\text{out}}(t,\omega) = \begin{bmatrix} S_{\text{out},11}(t,\omega) & S_{\text{out},12}(t,\omega) \\ S_{\text{out},21}(t,\omega) & S_{\text{out},22}(t,\omega) \end{bmatrix}, \tag{A.5}$$

where

$$\begin{aligned} S_{\text{out},11}(t,\omega) &= \frac{1}{\sqrt{2\pi}} \times \Big\{ \frac{-\kappa\epsilon}{4(\kappa+\epsilon)(\frac{\kappa}{2}+\frac{\epsilon}{2}-i\omega)}e^{-i\omega t} + \frac{\kappa\epsilon}{4(\kappa-\epsilon)(\frac{\kappa}{2}-\frac{\epsilon}{2}-i\omega)}e^{-i\omega t} \\ &+ \frac{-\kappa\epsilon}{4(\kappa+\epsilon)(\frac{\kappa}{2}+\frac{\epsilon}{2}+i\omega)}e^{-i\omega t} + \frac{\kappa\epsilon}{4(\kappa-\epsilon)(\frac{\kappa}{2}-\frac{\epsilon}{2}+i\omega)}e^{-i\omega t} + e^{-i\omega t} \\ &+ \xi^-_{\text{out}}(t)[\frac{(\epsilon^2+\kappa^2-4\gamma^2)\sqrt{2\gamma}}{(\epsilon+\kappa-2\gamma)(\epsilon-\kappa+2\gamma)(\gamma+i\omega)} + \frac{\kappa\sqrt{2\gamma}}{(\kappa+\epsilon-2\gamma)(\frac{\kappa}{2}+\frac{\epsilon}{2}+i\omega)} \\ &+ \frac{\kappa\sqrt{2\gamma}}{(\kappa-\epsilon-2\gamma)(\frac{\kappa}{2}-\frac{\epsilon}{2}+i\omega)}] + \xi^+_{\text{out}}(t)[\frac{2\kappa\epsilon\sqrt{2\gamma}}{(\epsilon+\kappa-2\gamma)(\epsilon-\kappa+2\gamma)(\gamma+i\omega)} \\ &- \frac{\kappa\sqrt{2\gamma}}{(\kappa+\epsilon-2\gamma)(\frac{\kappa}{2}+\frac{\epsilon}{2}+i\omega)} + \frac{\kappa\sqrt{2\gamma}}{(\kappa-\epsilon-2\gamma)(\frac{\kappa}{2}-\frac{\epsilon}{2}+i\omega)}]\Big\}, \\ S_{\text{out},12}(t,\omega) &= \frac{1}{\sqrt{2\pi}} \times \Big\{ \frac{\kappa\epsilon}{4(\kappa+\epsilon)(\frac{\epsilon}{2}+\frac{\kappa}{2}-i\omega)}e^{-i\omega t} + \frac{\kappa\epsilon}{4(\kappa-\epsilon)(\frac{\kappa}{2}-\frac{\epsilon}{2}-i\omega)}e^{-i\omega t} \\ &+ \frac{\kappa\epsilon}{4(\kappa+\epsilon)(\frac{\kappa}{2}+\frac{\epsilon}{2}+i\omega)}e^{-i\omega t} + \frac{\kappa\epsilon}{4(\kappa-\epsilon)(\frac{\kappa}{2}-\frac{\epsilon}{2}+i\omega)}e^{-i\omega t} \\ &+ \xi^-_{\text{out}}(t)[\frac{2\kappa\epsilon\sqrt{2\gamma}}{(\epsilon+\kappa-2\gamma)(\epsilon-\kappa+2\gamma)(\gamma+i\omega)} - \frac{\kappa\sqrt{2\gamma}}{(\kappa+\epsilon-2\gamma)(\frac{\kappa}{2}+\frac{\epsilon}{2}+i\omega)} \\ &+ \frac{\kappa\sqrt{2\gamma}}{(\kappa-\epsilon-2\gamma)(\frac{\kappa}{2}-\frac{\epsilon}{2}+i\omega)}] + \xi^+_{\text{out}}(t)[\frac{(\epsilon^2+\kappa^2-4\gamma^2)\sqrt{2\gamma}}{(\epsilon+\kappa-2\gamma)(\epsilon-\kappa+2\gamma)(\gamma+i\omega)} \\ &+ \frac{\kappa\sqrt{2\gamma}}{(\kappa+\epsilon-2\gamma)(\frac{\kappa}{2}+\frac{\epsilon}{2}+i\omega)} + \frac{\kappa\sqrt{2\gamma}}{(\kappa-\epsilon-2\gamma)(\frac{\kappa}{2}-\frac{\epsilon}{2}+i\omega)}]\Big\}, \\ S_{\text{out},21}(t,\omega) &= S_{\text{out},12}(t,\omega), \quad S_{\text{out},22}(t,\omega) = S_{\text{out},11}(t,\omega) - \frac{1}{\sqrt{2\pi}}e^{-i\omega t}. \end{aligned}$$